Mubbashar Nazeer*, Fayyaz Ahmad, Adila Saleem, Mubashara Saeed, Sidra Naveed, Mubarra Shaheen and Eman Al Aidarous

Effects of Constant and Space-Dependent Viscosity on Eyring–Powell Fluid in a Pipe: Comparison of the Perturbation and Explicit Finite Difference Methods

https://doi.org/10.1515/zna-2019-0095
Received March 25, 2019; accepted June 20, 2019; previously published online July 18, 2019

Abstract: The present study explores the effects of constant and space-dependent viscosity on Eyring–Powell fluid inside a circular pipe. The heat transfer analysis is also considered. Using the normalised quantities, the governing equations are transformed into dimensionless form, and then the solution of the constructed nonlinear differential equations is calculated. The perturbation method is used to find the analytical expressions of velocity and temperature profiles as a function of pipe radius. The perturbation solution is validated against explicit finite difference numerical method, and errors of each case are plotted. The accuracy in velocity and temperature of finite difference method relative to the perturbation method is of order 10^{-2} and 10^{-4}, respectively, in both cases of constant and space-dependent viscosity. The effects of various emerging parameters, namely, modified rheological parameter λ $(= 0.1)$, pressure gradient parameter G $(-1 \leq G \leq -0.4)$, rheological parameter ξ $(= 0.1)$ and material parameter E $(0.1 \leq E \leq 1)$ on temperature and velocity fields, are discussed through plots. The heights of both profiles are maximal for the case of constant model as compared to the variable one. The numerical code is also validated with a previous study of Eyring–Powell fluid in a pipe.

Keywords: Explicit Finite Difference Method; Eyring–Powell Fluid; Heat Transfer Analysis; Perturbation Method.

***Corresponding author: Mubbashar Nazeer,** Department of Mathematics, Riphah International University, Faisalabad Campus, Faisalabad 38000, Pakistan, E-mail: mubbashariiui@gmail.com. https://orcid.org/0000-0002-3932-6214
Fayyaz Ahmad, Adila Saleem, Mubashara Saeed, Sidra Naveed and Mubarra Shaheen: Department of Mathematics, Riphah International University, Faisalabad Campus, Faisalabad 38000, Pakistan
Eman Al Aidarous: Department of Mathematics, King Abdul Aziz University, Jeddah, Saudi Arabia

1 Introduction

The non-Newtonian fluids have been used in various investigations. Many authors have been using these fluids in different studies in various geometrical shapes due to the extensive role in engineering and industrial applications. Ice cream, apple sauce, soaps, muds sugar solution, various cosmetic products, animal blood, pulps, cheese, and so on may be added in the examples of non-Newtonian fluids. Many mathematical models are presented to represent the different features of various non-Newtonian fluids, since the equations of different non-Newtonian fluid models are more complicated as compared to equations of Newtonian fluid models. Due to this reason, mathematical modelling and solutions of these fluids equations are greatly significant. Even today, the great interest is noted in the development of mathematical modelling and solutions of non-Newtonian fluids [1, 2]. The Eyring–Powell fluid model has a fundamental importance in various chemical engineering processes and has a definite advantage over other non-Newtonian fluid models because of its simple modelling and ease of simulations. The Eyring–Powell fluid model is derived from the kinetic theory of liquids rather than empirical equation. Due to high and low shear stresses, it decorously transforms to viscous fluids (Newtonian fluids) [3]. A reasonable number of studies are cited in the next paragraph to highlight Eyring–Powell fluid and variable viscosity models in the previous literature.

Ali et al. [4] obtained the perturbation and numerical solutions of pressure-driven flow of an Eyring–Powell fluid inside the pipe. Hayat et al. [5] used the series solution method to find the solution of nonlinear-modelled equations of Eyring–Powell fluid and highlighted the important results. Hayat et al. [6] analysed the effects of magnetic field, heat generation/absorption, and thermal radiation on Eyring–Powell fluid over a stretching cylinder. Finite difference numerical technique was performed by Akbar et al. [7] to capture the effects of magnetic field on flow of Eyring–Powell fluid over a stretching surface. Nadeem and Saleem [8] employed the optimal homotopy

analysis method to solve the nonlinear partial differential equations of the Eyring–Powell fluid model and pointed out some useful results. The effects of physical parameters on magnetohydrodynamic (MHD) Eyring–Powell fluid over a rotating surface were investigated by Khan et al. [9]. Umavathi et al. [10] calculated the perturbation solution of mixed convection flow in two vertical channels under the effects of variable viscosity, thermal conductivity, and chemical reaction. They also compared their solution with the numerical iterative scheme and presented their error in tabular form. The effects of temperature-dependent viscosity with entropy generation on unsteady second-grade fluid over a vertical cylinder were investigated by Reddy et al. [11]. Sheremet et al. [12] reported the effects of inclined magnetic field and geothermal viscosity on free convection flow of Newtonian fluid inside the porous conduit. The effects of radiative heat flux on two-dimensional viscoelastic fluid inside the enclosure were investigated by Sheremet and Pop [13]. Applications of spectral method in MHD three-dimensional boundary layer flow (temperature-dependent viscosity) under the effects of viscous dissipation and Joule heating were presented by Turkyilmazoglu [14]. In other studies [15, 16], he presented the closed form solution of velocity and temperature of nanofluid into two different geometries (pipe and channel) and captured some important results under the effects of fluidic parameters.

In the present study, Eyring–Powell fluid inside the infinitely long pipe is considered. Such type of flow configuration is commonly used in polymeric liquids, slurries, food stuffs, and so on [17–19]. An Eyring–Powell fluid model is accommodated, while constant and space-dependent viscosity models are accounted in the current analysis. The analytical expressions for velocity and temperature profiles are presented. In this investigation, the motivation emanates from a desire to realise the effects of constant and space-dependent viscosity on Eyring–Powell fluid in a pipe. For cross-validation of analytically approximated solution obtained by the perturbation method, we will implement an explicit finite difference method to solve the same models. Here, the viscosity of the fluid depends upon space coordinate. The perturbation is used to find the analytical expressions of velocity and temperature profiles. The explicit finite difference method based on the Newton method [4, 20–31] is implemented to find the solution for the considered problem. The effects of controlling parameters on velocity and temperature profiles are pointed out. The important results of the present study are highlighted with the help of graphs.

2 Problem Formulation

Let us consider the steady-state, incompressible, one-dimensional flow of Eyring–Powell fluid inside an infinitely long pipe. The fluid is moving inside the pipe due to constant pressure gradient, and the viscosity of the fluid is taken as a constant and variable. The geometry of the present problem is shown in Figure 1. However, here the rheology of fluid flowing in the pipe is characterised by the Eyring–Powell model [1–4]. In particular, the analysis is carried out for two different viscosity models [17–19].

The Cauchy stress tensor for the current study is [3]

$$\mathbf{S} = \left[\mu + \frac{1}{K_2}\frac{Sinh^{-1}\left(K_3\dot{\psi}\right)}{\dot{\psi}}\right]\mathbf{A}_1, \tag{1}$$

where $\dot{\psi} = \sqrt{\frac{1}{2}tra\left(\mathbf{A}_1^2\right)}$.

Powell and Eyring [3] present the relation given in (1). With the help of $Sinh^{-1}$ approximation,

$$Sinh^{-1}\left(K_3\dot{\psi}\right) \cong K_3\dot{\psi} - \frac{1}{6}\left(K_3\dot{\psi}\right)^3, \quad \left|K_3\dot{\psi}\right| \ll 1. \tag{2}$$

The new form of (1) is

$$\mathbf{S} = \left[\mu + \mathrm{A} - \frac{B}{6}\dot{\psi}^2\right]\mathrm{A}_1, \quad B \ll 1, \tag{3}$$

where $\mathrm{A} = \frac{K_3}{K_2}$ and $\mathrm{B} = \frac{K_3^3}{K_2}$.

The velocity and temperature fields are defined by the given expression

$$\mathbf{V} = [0, 0, w(r)], \tag{4}$$

$$\theta = \theta(r). \tag{5}$$

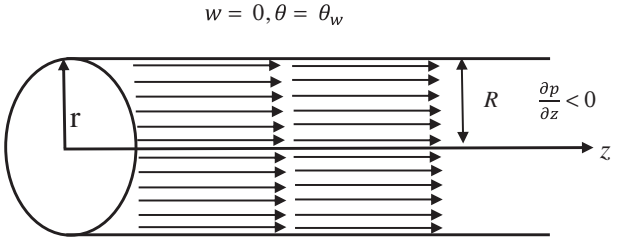

Figure 1: Geometry of the flow problem.

In view of (4), the stress tensor has the following form:

$$\mathbf{S} = \left(\mu + \mathrm{A} - \frac{B}{6}\left(\frac{\mathrm{d}w}{\mathrm{d}r}\right)^2\right)\begin{pmatrix} 0 & 0 & \left(\frac{\mathrm{d}w}{\mathrm{d}r}\right) \\ 0 & 0 & 0 \\ \left(\frac{\mathrm{d}w}{\mathrm{d}r}\right) & 0 & 0 \end{pmatrix}. \quad (6)$$

It is noted from the above equation, $S_{rz}(S_{zr})$ are only non-vanishing components of stress tensor $\mathbf{S}$

$$S_{rz} = S_{zr} = \left(\mu + A - \frac{B}{6}\left(\frac{\mathrm{d}w}{\mathrm{d}r}\right)^2\right)\left(\frac{\mathrm{d}w}{\mathrm{d}r}\right). \quad (7)$$

In the present situation, equations of continuity and conservation of momentum are given by

$$\frac{\partial w}{\partial z} = 0, \quad (8)$$

$$0 = -\frac{\partial p}{\partial z} + \frac{1}{r}\frac{\partial}{\partial r}(rS_{rz}), \quad (9)$$

substituting the values S_{rz} into (9), we have

$$\frac{1}{r}\frac{\mathrm{d}}{\mathrm{d}r}\left(\mu r\frac{\mathrm{d}w}{\mathrm{d}r}\right) + \frac{1}{r}\frac{\mathrm{d}}{\mathrm{d}r}\left(r\left(A\frac{\mathrm{d}w}{\mathrm{d}r} - \frac{B}{6}\left(\frac{\mathrm{d}w}{\mathrm{d}r}\right)^3\right)\right) = \frac{\mathrm{d}p}{\mathrm{d}z}. \quad (10)$$

The energy equations in the present problem take the following form:

$$\frac{\mu}{k}\left(\frac{\mathrm{d}w}{\mathrm{d}r}\right)^2 + \frac{A}{k}\left(\frac{\mathrm{d}w}{\mathrm{d}r}\right)^2 - \frac{B}{6k}\left(\frac{\mathrm{d}w}{\mathrm{d}r}\right)^4 + \frac{\mathrm{d}^2\theta}{\mathrm{d}r^2} + \frac{1}{r}\frac{\mathrm{d}\theta}{\mathrm{d}r} = 0. \quad (11)$$

The boundary conditions of (10) and (11) are

$$w = 0, \theta = \theta_w, \text{ at } r = R, \text{ and } \frac{\mathrm{d}w}{\mathrm{d}r} = \frac{\mathrm{d}\theta}{\mathrm{d}r} = 0 \text{ at } r = 0. \quad (12)$$

With the help of normalised quantities [4], the new forms of (10–12) are

$$\frac{\mathrm{d}\mu}{\mathrm{d}r}\frac{\mathrm{d}w}{\mathrm{d}r} + \frac{\mu}{r}\left(\frac{\mathrm{d}w}{\mathrm{d}r} + r\frac{\mathrm{d}^2w}{\mathrm{d}r^2}\right) + \frac{E}{r}\left(\frac{\mathrm{d}w}{\mathrm{d}r} + r\frac{\mathrm{d}^2w}{\mathrm{d}r^2}\right) - \frac{\zeta E}{r}\left(\frac{\mathrm{d}w}{\mathrm{d}r}\right)^2\left(\frac{\mathrm{d}w}{\mathrm{d}r} + 3r\frac{\mathrm{d}^2w}{\mathrm{d}r^2}\right) = G \quad (13)$$

$$\eta\left(\frac{\mathrm{d}w}{\mathrm{d}r}\right)^2\left(\mu + E - E\zeta\left(\frac{\mathrm{d}w}{\mathrm{d}r}\right)^2\right) + \frac{\mathrm{d}^2\theta}{\mathrm{d}r^2} + \frac{1}{r}\frac{\mathrm{d}\theta}{\mathrm{d}r} = 0 \quad (14)$$

$$w(r=1) = 0, \ \theta(r=1) = 0, \text{ and } \frac{\mathrm{d}w(r=0)}{\mathrm{d}r} = \frac{\mathrm{d}\theta(r=0)}{\mathrm{d}r} = 0 \quad (15)$$

where

$\theta =$ dimensionless temperature
$w =$ dimensionless velocity component along z axis
$\mu =$ dimensionless viscosity
$r =$ dimensionless radius

$$G = \frac{\partial p}{\partial z}\frac{R^2}{\mu_0 w_0}.$$
$$\zeta = \frac{k_3^2 w_0^2}{6\mu_0 R^2}$$
$$E = \frac{A}{\mu_0}.$$
$$\lambda = \frac{Ak_3^2 w_0^2}{6\mu_0^2 R^2}$$
$$\eta = \frac{\mu_0 w_0^2}{k(\theta_m - \theta_w)}.$$

The solution is presented here for two different viscosity models.

2.1 Constant Viscosity Model

In the case of constant viscosity model, we choose $\mu = 1$ and (13–15) take the following form:

$$\left(\frac{\mathrm{d}w}{\mathrm{d}r} + r\frac{\mathrm{d}^2w}{\mathrm{d}r^2}\right) + E\left(\frac{\mathrm{d}w}{\mathrm{d}r} + r\frac{\mathrm{d}^2w}{\mathrm{d}r^2}\right) - \lambda\left(\frac{\mathrm{d}w}{\mathrm{d}r}\right)^2\left(\frac{\mathrm{d}w}{\mathrm{d}r} + 3r\frac{\mathrm{d}^2w}{\mathrm{d}r^2}\right) = Gr \quad (16)$$

$$\frac{\mathrm{d}^2\theta}{\mathrm{d}r^2} + \frac{1}{r}\frac{\mathrm{d}\theta}{\mathrm{d}r} + \eta\left(\frac{\mathrm{d}w}{\mathrm{d}r}\right)^2\left(1 + E - \lambda\left(\frac{\mathrm{d}w}{\mathrm{d}r}\right)^2\right) = 0 \quad (17)$$

$$w(r=1) = 0, \ \theta(r=1) = 0, \text{ and } \frac{\mathrm{d}w(r=0)}{\mathrm{d}r} = \frac{\mathrm{d}\theta(r=0)}{\mathrm{d}r} = 0 \quad (18)$$

To solve (16–18), let us assume $\lambda = \epsilon\Lambda$. The two-term perturbation expansions for velocity and temperature are defined by

$$w \sim w_0 + \epsilon w_1 + O\left(\epsilon^2\right) \quad (19a)$$

and

$$\theta \sim \theta_0 + \epsilon\theta_1 + O\left(\epsilon^2\right) \quad (19b)$$

where ϵ is known as perturbation parameter ($0 < \epsilon \ll 1$). In view of the above expansion, we have:

System of velocity for each order of ϵ is

$$\textit{order of one}: \ r\frac{\mathrm{d}^2w_0}{\mathrm{d}r^2} + \frac{\mathrm{d}w_0}{\mathrm{d}r} = \frac{Gr}{(1+E)}, \quad (20a)$$

$$w_0(r=1)=0, \quad \frac{\mathrm{d}w_0(r=0)}{\mathrm{d}r}=0, \tag{20b}$$

$$\textit{order of } \epsilon\text{: } r\frac{\mathrm{d}^2w_1}{\mathrm{d}r^2}+\frac{\mathrm{d}w_1}{\mathrm{d}r} = \frac{\Lambda}{(1+E_1)}\left(\frac{\mathrm{d}w_0}{\mathrm{d}r}\right)^2\left(\frac{\mathrm{d}w_0}{\mathrm{d}r}+3r\frac{\mathrm{d}^2w_0}{\mathrm{d}r^2}\right), \tag{20c}$$

$$w_1(r=1)=0, \quad \frac{\mathrm{d}w_1(r=0)}{\mathrm{d}r}=0. \tag{20d}$$

System of temperature for each order of ϵ is

$$\frac{\mathrm{d}^2\theta_0}{\mathrm{d}r^2}+\frac{1}{r}\frac{\mathrm{d}\theta_0}{\mathrm{d}r}=-\eta(1+E)\left(\frac{\mathrm{d}w_0}{\mathrm{d}r}\right)^2, \tag{21a}$$

$$\theta_0(r=1)=0, \quad \frac{\mathrm{d}\theta_0(r=0)}{\mathrm{d}r}=0, \tag{21b}$$

$$\frac{\mathrm{d}^2\theta_1}{\mathrm{d}r^2}+\frac{1}{r}\frac{\mathrm{d}\theta_1}{\mathrm{d}r} = -\eta\left(2(1+E)\left(\frac{\mathrm{d}w_1}{\mathrm{d}r}\right)\left(\frac{\mathrm{d}w_0}{\mathrm{d}r}\right)-\Lambda\left(\frac{\mathrm{d}w_0}{\mathrm{d}r}\right)^4\right), \tag{21c}$$

$$\theta_1(r=1)=0, \quad \frac{\mathrm{d}\theta_1(r=0)}{\mathrm{d}r}=0. \tag{21d}$$

The solutions of each order of ϵ for velocity profile are

$$w_0=\frac{-G\left(1-r^2\right)}{4(1+E)} \tag{22a}$$

$$w_1=\frac{G^3\Lambda\left(-1+r^4\right)}{32(1+E)^4} \tag{22b}$$

Based on the leading-order solution, the determining equations for the correction term give

$$\theta_0=\frac{G^2\,\eta}{64(1+E)}\left(1-r^4\right) \tag{23a}$$

$$\theta_1=-\frac{\eta\,\Lambda\,G^4\left(-1+r^6\right)}{576(1+E)^4} \tag{23b}$$

Combining the leading-order and first-order solutions, we get

$$w=\frac{-G}{4(1+E)}\left(1-r^2\right)+\frac{\lambda\,G^3}{32(1+E)^4}\left(r^4-1\right), \tag{24}$$

$$\theta=\frac{G^2\,\eta}{64(1+E)}\left(1-r^4\right)-\frac{\lambda\,G^4\,\eta}{576(1+E)^4}\left(-1+r^6\right), \tag{25}$$

2.2 Space-Dependent Viscosity Model

According to Ellahi and Riaz [18] and Hayat et al. [19], $\mu=r$; therefore, the new forms of (13–14) are

$$\left(E\,r+r^2\right)\left(\frac{\mathrm{d}^2w}{\mathrm{d}r^2}\right)+(E+2\,r)\left(\frac{\mathrm{d}w}{\mathrm{d}r}\right) -\zeta E\left(\frac{\mathrm{d}w}{\mathrm{d}r}\right)^2\left(\frac{\mathrm{d}w}{\mathrm{d}r}+3\,r\frac{\mathrm{d}^2w}{\mathrm{d}r^2}\right)=G\,r \tag{26}$$

$$\frac{\mathrm{d}^2\theta}{\mathrm{d}r^2}+\frac{1}{r}\frac{\mathrm{d}\theta}{\mathrm{d}r} +\eta\left(\frac{\mathrm{d}w}{\mathrm{d}r}\right)^2\left((r+E)-E\,\zeta\left(\frac{\mathrm{d}w}{\mathrm{d}r}\right)^2\right)=0 \tag{27}$$

System of velocity for each order of ϵ is

$$\textit{order of one}\text{: } \left(E\,r+r^2\right)\frac{\mathrm{d}^2w_0}{\mathrm{d}r^2}+(E+2r)\frac{\mathrm{d}w_0}{\mathrm{d}r}=G\,r \tag{28a}$$

$$w_0(r=1)=0, \quad \frac{\mathrm{d}w_0(r=0)}{\mathrm{d}r}=0, \tag{28b}$$

$$\textit{order of } \epsilon\text{: } \left(E\,r+r^2\right)\frac{\mathrm{d}^2w_1}{\mathrm{d}r^2}+(E+2r)\frac{\mathrm{d}w_1}{\mathrm{d}r} = -E\Lambda\left(\frac{\mathrm{d}w_0}{\mathrm{d}r}\right)^2\left(\frac{\mathrm{d}w_0}{\mathrm{d}r}+3\,r\frac{\mathrm{d}^2w_0}{\mathrm{d}r^2}\right) \tag{28c}$$

$$w_1(r=1)=0, \quad \frac{\mathrm{d}w_1(r=0)}{\mathrm{d}r}=0. \tag{28d}$$

System of temperature for each order of ϵ is

$$\frac{\mathrm{d}^2\theta_0}{\mathrm{d}r^2}+\frac{1}{r}\frac{\mathrm{d}\theta_0}{\mathrm{d}r}=-\Lambda(1+E)\left(\frac{\mathrm{d}w_0}{\mathrm{d}r}\right)^2, \tag{29a}$$

$$\theta_0(r=1)=0, \quad \frac{\mathrm{d}\theta_0(r=0)}{\mathrm{d}r}=0, \tag{29b}$$

$$\frac{\mathrm{d}^2\theta_1}{\mathrm{d}r^2}+\frac{1}{r}\frac{\mathrm{d}\theta_1}{\mathrm{d}r} = -\eta\left(2(1+E)\left(\frac{\mathrm{d}w_1}{\mathrm{d}r}\right)\left(\frac{\mathrm{d}w_0}{\mathrm{d}r}\right)-E\Lambda\left(\frac{\mathrm{d}w_0}{\mathrm{d}r}\right)^4\right), \tag{29c}$$

$$\theta_1(r=1)=0, \quad \frac{\mathrm{d}\theta_1(r=0)}{\mathrm{d}r}=0. \tag{29d}$$

The solutions of each order of ϵ for velocity profile are

$$w_0 = -\frac{G}{2}(1-r) + \frac{G\,E}{2}\log\left(\frac{1+E}{E+r}\right) \tag{30a}$$

$$\begin{aligned} w_1 = \Lambda\Bigg(&-\frac{G^3E^2(18+E(27+11E))}{48(1+E)^3} \\ &+\frac{G^3E^2\left(11E^2+27E\,r+18r^2\right)}{48(E+r)^3} \\ &+\frac{1}{8}G^3E\log\left(\frac{E+r}{1+E}\right)\Bigg) \end{aligned} \tag{30b}$$

Based on the leading-order solution, the determining equations for correction term give

$$\begin{aligned} \theta_0 = &\frac{\eta\,G^2}{144}\left(4-4r^3-9E\left(1-r^2\right)\right)+\frac{\eta\,G^2E^2}{4}(1-r) \\ &+\frac{\eta\,G^2E^3}{4}\left(Li_2\left(-\frac{1}{E}\right)-Li_2\left(-\frac{r}{E}\right)\right) \end{aligned} \tag{31a}$$

$$\begin{aligned} \theta_1 = &\frac{G^4E\,\eta\,\Lambda\left(-1+(1+E)^2r^2\right)}{64(1+E)^2} \\ &-\frac{G^4E^2\eta\Lambda\left(-7+8(1+E)^2r\right)}{32(1+E)^2} \\ &+\frac{G^4E^4\,\eta\,\Lambda}{96}\left(\frac{37}{(1+E)^2}-\frac{13}{E+r}\right) \\ &+\frac{\eta\,\Lambda\,G^4E^3}{192}\left(\frac{3\left(31+8E^2\right)}{(1+E)^2}+\frac{2E^2}{(E+r)^2}\right) \\ &+\frac{47\,G^4E^3\,\eta\,\Lambda}{96}\left(\log\left[\frac{1+E}{E+r}\right]\right) \\ &+\frac{5G^4\,E^3\,\eta\,\Lambda}{8}\left(Li_2\left(-\frac{1}{E}\right)-Li_2\left(-\frac{r}{E}\right)\right) \end{aligned} \tag{31b}$$

Combining the leading-order and first-order solutions, we get

$$\begin{aligned} w = &-\frac{G}{2}(1-r)+\frac{G\,E}{2}\log\left(\frac{1+E}{E+r}\right) \\ &-\xi\left(\begin{array}{l} \dfrac{G^3E^2(18+E(27+11E))}{48(1+E)^3} \\ \quad+\dfrac{1}{8}G^3E\log\left(\dfrac{E+r}{1+E}\right) \\ \quad+\dfrac{G^3E^2\left(11E^2+27E\,r+18r^2\right)}{48(E+r)^3} \end{array}\right) \end{aligned} \tag{32}$$

$$\begin{aligned} \theta = &\frac{\eta\,G^2}{144}\left(4-4r^3-9E\left(1-r^2\right)\right)+\frac{\eta\,G^2E^2}{4}(1-r) \\ &+\frac{\eta\,G^2E^3}{4}\left(Li_2\left(-\frac{1}{E}\right)-Li_2\left(-\frac{r}{E}\right)\right) \\ &+\eta\xi\left(\begin{array}{l} \dfrac{G^4E\left(-1+(1+E)^2r^2\right)}{64(1+E)^2} \\ -\dfrac{G^4E^2\left(-7+8(1+E)^2r\right)}{32(1+E)^2} \\ +\dfrac{G^4E^4}{96}\left(\dfrac{37}{(1+E)^2}-\dfrac{13}{E+r}\right) \\ +\dfrac{G^4E^3}{192}\left(\dfrac{3\left(31+8E^2\right)}{(1+E)^2}+\dfrac{2E^2}{(E+r)^2}\right) \\ +\dfrac{47\,G^4E^3}{96}\left(\log\left[\dfrac{1+E}{E+r}\right]\right) \\ +\dfrac{5G^4\,E^3}{8}\left(Li_2\left(-\frac{1}{E}\right)-Li_2\left(-\frac{r}{E}\right)\right) \end{array}\right), \end{aligned} \tag{33}$$

where, $Li_2(\chi)$ denotes the second-order polylogarithmic function, which is defined by

$$Li_2(\chi) = -\int_0^{\chi}\frac{\ln(1-l)}{l}\mathrm{d}l. \tag{34}$$

3 Finite Difference Method

To cross the numerical results, we discretise the given mathematical model by using explicit finite difference method. The discretisation of domain [0, 1] can be performed by

$$r_i = r_1 + (i-1)h, \quad \text{for } i = 1, 2, 3, \ldots, n, \tag{35}$$

where $h = 1/(n-1)$ and $r_1 = 0$. For the description of stencils, we take y as a function of r, i.e. $y \equiv y(r)$. The finite difference stencils for first- and second-order derivatives can be written as

$$y'_1 = \left[-\frac{1}{h}, 0, \frac{1}{h}\right]\begin{bmatrix} y_{i-1} \\ y_i \\ y_{i+1}\end{bmatrix} + O\left(h^2\right), \tag{36a}$$

$$y''_1 = \left[-\frac{1}{h^2}, \frac{-2}{h^2}, \frac{1}{h^2}\right]\begin{bmatrix} y_{i-1} \\ y_i \\ y_{i+1}\end{bmatrix} + O\left(h^2\right), \tag{36b}$$

where $y_i = y(r_i)$, $y'_i = y'(r_i)$, $y''_i = y''(r_i)$ and $i = 2, 3, \ldots, n-1$. We observe the following boundary condition:

$$y'(r_i) = 0,$$
$$y(r_n) = 0. \tag{37}$$

Stencil for one-sided first-order derivative, which is also second-order accurate, is

$$y'_i = \left[-\frac{3}{(2h)}, \frac{2}{h}, \frac{-1}{(2h)}\right] \begin{bmatrix} y_1 \\ y_2 \\ y_3 \end{bmatrix} + O\left(h^2\right), \tag{38}$$

To implement boundary condition at r_1, we get

$$\frac{-3}{2h} y_1 + \frac{2}{h} y_2 - \frac{1}{2h} y_3 = 0, \tag{39}$$

which gives us

$$-3y_1 + 4y_2 - y_3 = 0. \tag{40}$$

The applications of these finite difference schemes to (13) and (14) for the first case and (16) and (17) for the second case give us a system of nonlinear equations that incorporate boundary conditions as well. We use the Newton method to solve the system of nonlinear equations.

4 Code Validation

In this section, we have validated our implicit finite difference numerical code with the perturbation solution of Akinshilo and Olaye [32] for both velocity and temperature fields. With our numerical code, we have solved (1) and (2) of Akinshilo and Olaye [32] for the flow of Eyring–Powell fluid in a pipe under the effects of heat generation and variable viscosity models. The results are presented in the form of velocity and temperature profiles for the case of Reynolds viscosity model (in the absence of heat generation) in Figure 2. From Figure 2, it is noted that our solution is well agreed with the perturbation solution of Akinshilo and Olaye [32].

5 Results and Discussion

We examine the effects of pertinent parameters on the velocity and temperature profiles emerging in the steady flows of Eyring–Powell fluid in the pipe under the two famous models of viscosity, namely, constant viscosity model and space-dependent viscosity model, respectively. For this purpose, the authors have drawn Figures 3–10

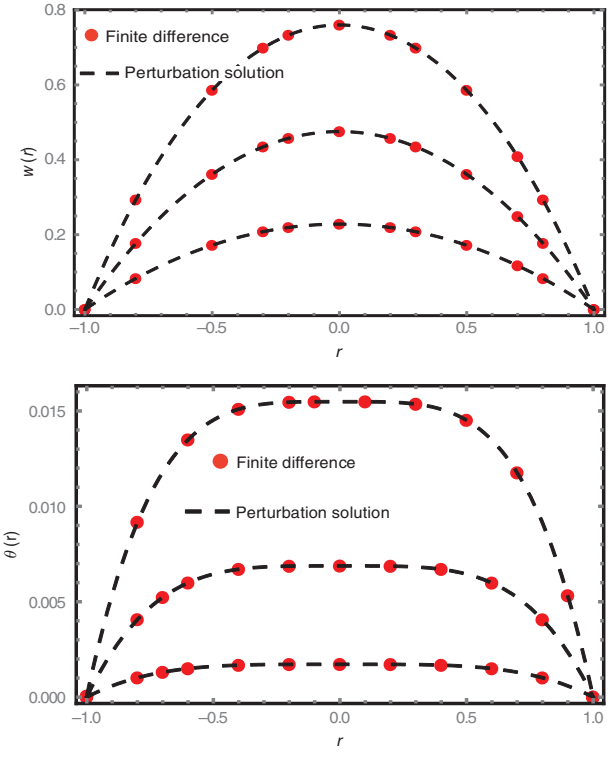

Figure 2: w and θ versus E, respectively, when $G = -1, -2, -3$, $E = 0.1$, $\eta = -0.1$, $\lambda = 0.1$.

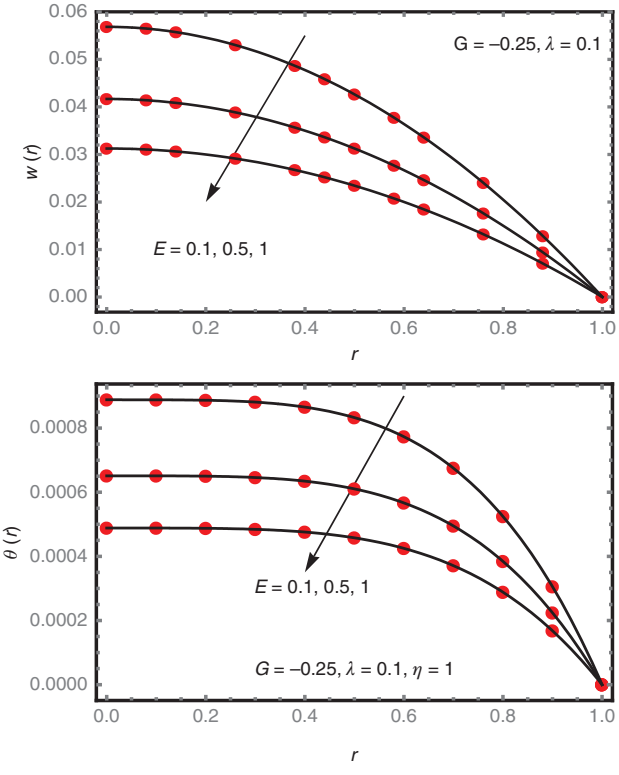

Figure 3: Comparison with Akinshilo and Olaye [32]. w and θ versus E, respectively.

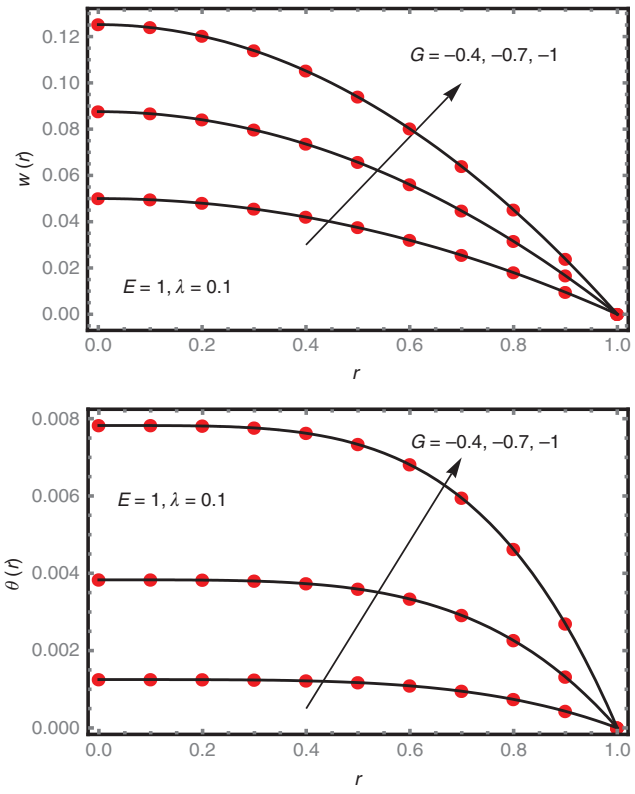

Figure 4: Constant viscosity case: w and θ versus G, respectively.

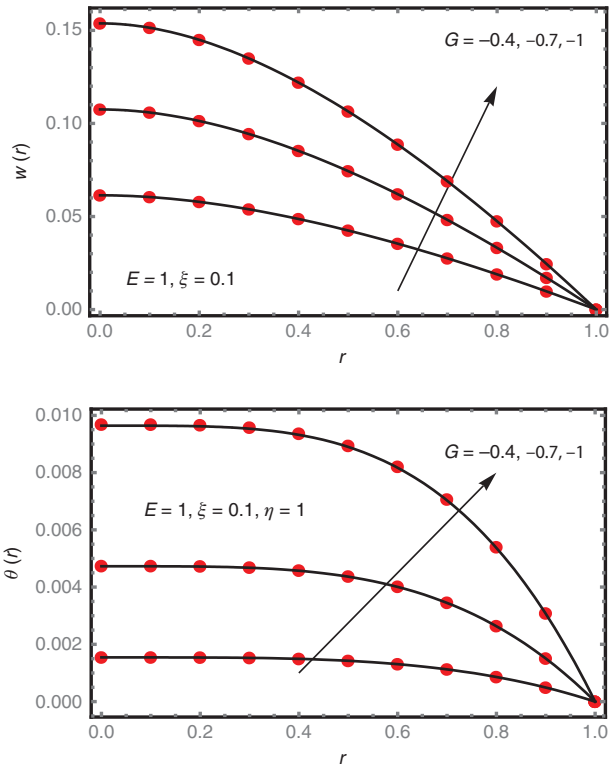

Figure 6: Space-dependent viscosity case: w and θ versus G, respectively.

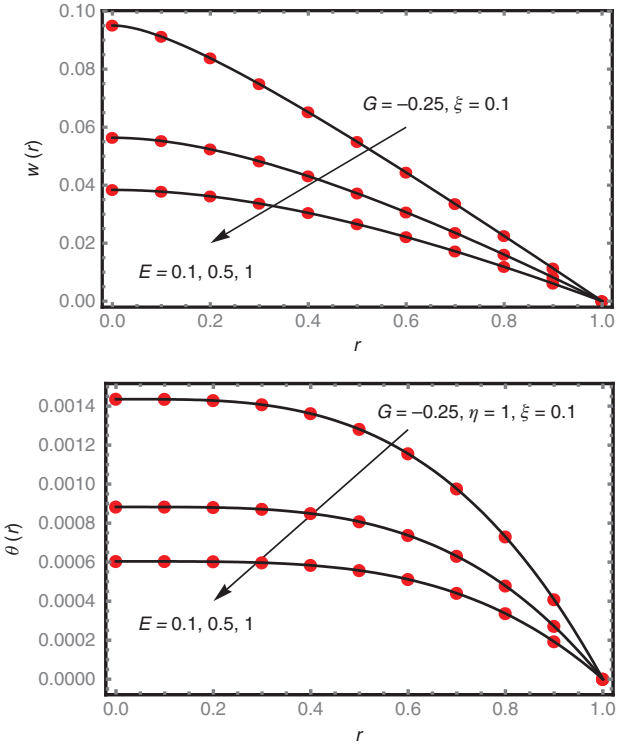

Figure 5: Constant viscosity case: w and θ versus E, respectively.

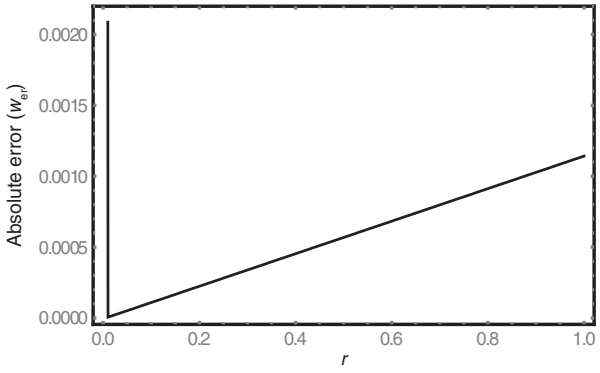

Figure 7: Error of velocity profile for the first case.

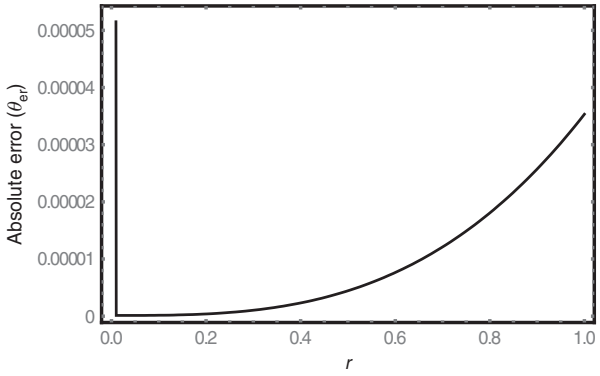

Figure 8: Error of temperature profile for the first case.

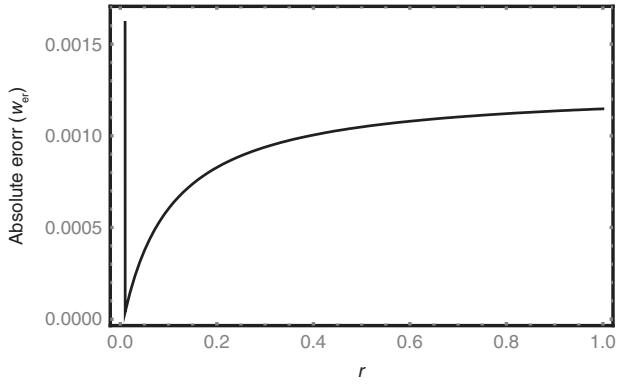

Figure 9: Error of velocity profile for the second case.

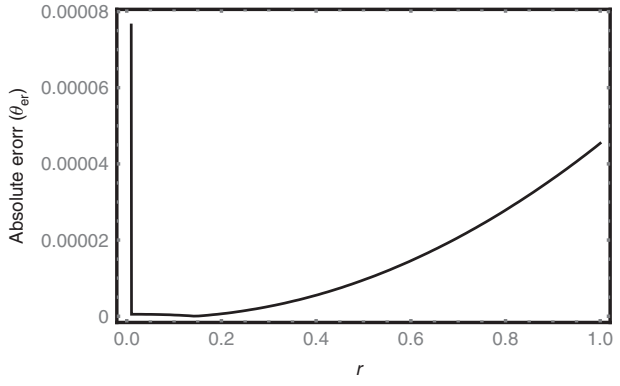

Figure 10: Error of temperature profile for the second case.

with the help of perturbation and finite difference solutions against the pipe radius. The effects of physical parameters on velocity and temperature profiles are discussed through graphs separately for both cases. The physical parameters and their ranges are chosen on the basis of the previous studies [4, 19, 32, 33] on non-Newtonian fluids. The modified rheological parameter λ and rheological parameter ξ are selected 0.1 throughout the study, while the other physical parameters, namely, pressure gradient parameter G and material parameter E, are, respectively, $-1 \leq G \leq -0.4$ and $0.1 \leq E \leq 1$.

Figures 3 and 4 are constructed for constant viscosity model, and Figures 5 and 6 for space-dependent viscosity model, respectively. In each figure, solid lines indicate the perturbation solution, while solid circles show the numerical solution, which is obtained by finite difference scheme. Figure 3 depicts the effects of Eyring–Powell parameter on velocity and temperature profiles. It is noted that the velocity and temperature profiles decrease with increasing the values of material parameter E. The effects of pressure gradient parameter G on both profiles are shown in Figure 4. From the figure, it is observed that the velocity and temperature fields increase with increasing the pressure gradient parameter G. The effects of E on velocity and temperature profiles for the case of space-dependent viscosity are displayed in Figure 5. The velocity and temperature profiles also have a decreasing behaviour against material parameter E. It is noted that the profiles of velocity and temperature in space-dependent viscosity model are higher than the case of constant viscosity model. Figure 6 describes the characteristics of pressure gradient parameter G on velocity and temperature profiles for the case of variable viscosity model. The effects are the same on the velocity and temperature fields of E as we discussed in the previous model (Fig. 4), except that the height of the profiles is maximum from the first case. Basically, it is observed that the same observations are noted qualitatively in both profiles against all emerging parameters for both considered cases except for the small difference quantitatively.

6 Error Magnitude

We compare the solutions obtained by the perturbation method and explicit finite difference method. By taking 100 grid points, we plotted the absolute differences of velocity and temperature profiles for cases 1 and 2 in Figures 7–10, respectively. The absolute difference of velocities and temperatures in both cases is of the order 10^{-2} and 10^{-4}, respectively.

7 Conclusions

In the present article, we consider the flow of the Eyring–Powell fluid model in the pipe whose viscosity is constant and space dependent. Here, we discussed the time-independent flow in a pipe due to constant pressure gradient. The analytical solution is obtained with the help of the perturbation method for both viscosity models. The numerical solution is also obtained with the help of eminent explicit finite difference scheme, and it was also compared with the perturbation solution for cross-validation. The orders of error of finite difference method relative to the perturbation method, in both cases, are 10^{-2} and 10^{-4} in velocities and temperatures, respectively. With the help of graphs, the effects of controlling parameters on the velocity and temperature fields are analysed. The analytical solution for the case of variable viscosity of the Eyring–Powell fluid model is presented here for the first time in literature. It is confirmed that, although the numerical iterative methods provide the optimal solutions for extensive range of controlling parameters, they did not provide the

analytical expression of velocity and temperature profiles. If the experimental data are available for controlling the parameters of Eyring–Powell fluid, then these analytical expressions of the velocity and temperature fields are beneficial in the future. Further, the solution of our study can be useful in the applications of engineering.

Nomenclature

R	Radius of pipe
E	Material parameter
λ	Modified rheological parameter
G	Pressure gradient parameter
ξ	Rheological parameter
θ_m	Bulk means fluid temperature
μ	Viscosity of the fluid
S	Cauchy stress tensor
K_2, K_3	Material constants
A_1	Rivlin–Ericksen tensor
w	Velocity components along z direction
r	Dimensionless radius
θ	Temperature of the fluid
θ_w	Wall's temperature
k	Thermal conductivity
w_0	Reference velocity
p	Pressure of the fluid
μ	Viscosity of the fluid
ϵ	Perturbation parameter
η	Related to Prandtl and Eckert number

References

[1] T. Hayat, S. Makhdoom, M. Awais, S. Saleem, and M. M. Rashidi, Appl. Math. Mech. **37**, 919 (2016).
[2] Z. Abbas, M. Sheikh, and S. S. Motsa, Energy **95**, 12 (2016).
[3] R. E. Powell and H. Eyring, Nature **154**, 427 (1944).
[4] N. Ali, F. Nazeer, and M. Nazeer, Z. Naturforsch. A **73**, 265 (2018).
[5] T. Hayat, M. Awais, and S. Asghar, J. Egyptian Math. Soc. **21**, 379 (2013).
[6] T. Hayat, M. I. Khan, M. Waqas, and A. Alsaedi, J. Mol. Liq. **231**, 126 (2017).
[7] N. S. Akbar, A. Ebaid, and Z. H. Khan, J. Magn. Magn. Mater. **382**, 355 (2015).
[8] S. Nadeem and S. Saleem, Results Phys. **4**, 54 (2014).
[9] N. A. Khan, S. Aziz, and N. A. Khan, J. Taiwan Inst. Chem. Eng.**45**, 2859 (2014).
[10] J. C. Umavathi, M. A. Sheremet, and S. Mohiuddin, Eur. J. Mech. B. Fluids **58**, 98 (2016).
[11] G. J. Reddy, M. Kumar, J. C. Umavathi, and M. A. Sheremet, Can. J. Phys. **96**, 978 (2018).
[12] M. A. Sheremet, M. S. Astanina, and I. Pop, Int. J. Numer. Methods Heat Fluid Flow **28**, 2111 (2018).
[13] M. A. Sheremet and I. Pop, Int. J. Numer. Methods Heat Fluid Flow **28**, 624 (2018).
[14] M. Turkyilmazoglu, Int. J. Therm. Sci. **49**, 563 (2010).
[15] M. Turkyilmazoglu, Int. J. Heat Mass Transfer **85**, 609 (2015).
[16] M. Turkyilmazoglu, Int. J. Heat Mass Transfer **126**, 974 (2018).
[17] R. Ellahi, E. Shivanian, S. Abbasbandy, and T. Hayat, Int. J. Numer. Methods Heat Fluid Flow **26**, 1433 (2016).
[18] R. Ellahi and A. Riaz, Math. Comput. Model. **52**, 1783 (2010).
[19] T. Hayat, R. Ellahi, and S. Asghar, Commun. Nonlinear Sci. Numer. Simul. **12**, 300 (2007).
[20] R. Ellahi, Appl. Math. Model. **37**, 1451 (2013).
[21] A. Majeed, T. Javed, and A. Ghaffari, Can. J. Phys. **95**, 969 (2017).
[22] M. Nazeer, N. Ali, and T. Javed, Can. J. Phys. **96** (6), 576 (2018).
[23] N. Ali, M. Nazeer, T. Javed, and M. A. Siddiqui, Heat Trans. Res. **49**, 457 (2018).
[24] M. Nazeer, N. Ali, and T. Javed, Int. J. Numer. Methods Heat Fluid Flow **28** (10), 2404 (2018).
[25] N. Ali, M. Nazeer, T. Javed, and F. Abbas, Meccanica **53**, 3279 (2018).
[26] M. Nazeer, N. Ali, and T. Javed, J. Porous Media **21**, 953 (2018).
[27] M. Nazeer, N. Ali, T. Javed, and Z. Asghar, Eur. Phys. J. Plus **133**, 423 (2018).
[28] M. Nazeer, N. Ali, and T. Javed, Can. J. Phys. **97**, 1 (2019).
[29] N. Ali, M. Nazeer, T. Javed, and M. Razzaq, Eur. Phys. J. Plus **2**, 134 (2019).
[30] M. Nazeer, N. Ali, T. Javed, and M. Razzaq, Int. J. Hydrog. Energy **44**, 953 (2019).
[31] M. Nazeer, N. Ali, T. Javed, and M. W. Nazir, Eur. Phys. J. Plus **134**, 204 (2019).
[32] A. T. Akinshilo and O. Olaye, J. King Saud Univ., Eng. Sci. **31**, 271 (2019).
[33] A. Hussain, M. Y. Malik, and F. Khan, Chin. J. Eng. **1**, 1 (2013).